



# Modulation of inflammation and angiogenesis and changes in ECM GAG-activity via dual delivery of nucleic acids



Shane Browne <sup>a</sup>, Michael G. Monaghan <sup>b</sup>, Eva Brauchle <sup>b</sup>, Daniel Carvajal Berrio <sup>b</sup>, Sandrine Chantepie <sup>c</sup>, Dulce Papy-Garcia <sup>c</sup>, Katja Schenke-Layland <sup>b, d, e</sup>, Abhay Pandit <sup>a, \*</sup>

<sup>a</sup> Centre for Research in Medical Devices (CÚRAM), National University of Ireland Galway, Ireland

<sup>b</sup> Department of Cell and Tissue Engineering, Fraunhofer Institute for Interfacial Engineering and Biotechnology, Stuttgart, Germany

<sup>c</sup> Laboratoire Croissance Cellulaire, Réparation et Régénération Tissulaires, CRRET/EA-4397/CNRS ERL-9215, Université Paris Est Créteil, Université Paris Est, F-94000, Créteil, France

<sup>d</sup> Dept. of Women's Health, Research Institute for Women's Health, Eberhard Karls University, Tübingen, Germany

<sup>e</sup> Department of Medicine/Cardiology, Cardiovascular Research Laboratories, University of California, Los Angeles, CA, USA

## ARTICLE INFO

### Article history:

Received 5 May 2015

Received in revised form

4 August 2015

Accepted 5 August 2015

Available online 6 August 2015

### Keywords:

Collagen

Gene therapy

Inflammation

Angiogenesis

Extracellular matrix (ECM)

## ABSTRACT

Tissue-engineered organs and implants hold promise for the replacement of damaged and diseased organs. However, the foreign body response (FBR) is a major obstacle that compromises the function of tissue-engineered constructs, typically causing them to fail. Two components of FBR are an inflammatory response and a lack of vascularization. To overcome these limitations, a collagen system was developed to release interleukin-6 (IL-6) siRNA and endothelial nitric oxide synthase (eNOS) pDNA in a staggered manner. Hollow collagen microspheres were assembled into a collagen sphere-in-hydrogel system that displayed a staggered release profile *in vitro*. This system was assessed *in vivo* in a subcutaneous rat model. The doses of IL-6 siRNA and eNOS pDNA were first individually optimized for their ability to reduce the volume fraction of inflammatory cells (7 days) and increase the length density of blood vessels (14 days), respectively. The identified optimal doses were combined, and the ability of the system to decrease the volume fraction of inflammatory cells and increase the length density of blood vessels was confirmed at both 7 and 14 days. Analysis of the tissue using Raman microspectroscopy revealed that in addition to changes in inflammation and angiogenesis, there were also changes in the extracellular matrix (ECM) at seven days. While changes in sulfated glycosaminoglycan (sGAG) content of the ECM were not detected, changes in the binding of sGAG of the ECM to growth factors were observed. Two growth factors tested, VEGF<sub>165</sub> and bFGF showed increased binding to sGAG extracted from eNOS pDNA-treated samples at seven days, increasing the angiogenic potential of the ECM. Thus, we observe that changes in the tissue in terms of the balance of inflammation and angiogenesis as well changes in the activity of sGAG of the ECM occurs following dual delivery of nucleic acids from the collagen sphere-in-hydrogel system.

© 2015 Elsevier Ltd. All rights reserved.

## 1. Introduction

Biomaterials comprise a key element of tissue engineering and regenerative medicine strategies [1–3] intended to aid in the repair and regeneration of tissue by facilitating the attachment, proliferation and differentiation of cells by providing a structural support [3,4]. In this respect, extracellular matrix (ECM)-based biomaterials have attracted great interest, particularly those derived from

collagens [5]. Collagens are the primary ECM components of many tissues including skin, tendon and blood vessels. Collagens are highly conserved between species, and when used as a biomaterial, have a close resemblance to the natural ECM. In addition, collagens, especially collagen type I, are amenable to functionalization with bioactive agents [6].

Despite its widespread use *in vivo*, collagen-based biomaterials elicit a foreign body response (FBR) following implantation [7–9]. The FBR is the host's immune response to the implantation of a foreign material. The FBR comprises an initial inflammatory reaction characterized by the presence of neutrophils and

\* Corresponding author.

E-mail address: [abhay.pandit@nuigalway.ie](mailto:abhay.pandit@nuigalway.ie) (A. Pandit).

macrophages, which initiates the formation of an immature vascular network [10]. These two key processes, inflammation and angiogenesis, are intimately related and share a temporal overlap [11,12]. Thus, an approach that appreciates the complex relationship between inflammation and angiogenesis is essential. A means by which one can appropriately modify the balance between inflammation and angiogenesis in the FBR will be useful for implantable biomaterials and tissue engineered constructs alike.

Attempts to modulate the FBR have involved the delivery of a single factor, typically an anti-inflammatory agent or a pro-angiogenic agent, such as dexamethasone [13] or VEGF [14]. However, modification of either process can compromise the other. This was illustrated when delivery of an interleukin-10 (IL-10) encoding pDNA via a hexamethylenediisocyanate-crosslinked collagen type I disc resulted in a reduction of not only inflammation but also angiogenesis at 21 days [15]. Conversely, the delivery of two angiogenic growth factors, fibroblast growth factor (FGF) and vascular endothelial growth factor (VEGF), enhanced the FBR to an implanted vascular graft, with evidence of giant cells and graft encapsulation [16]. Further evidence exists that growth factors such as FGF and VEGF, typically associated with the promotion of endothelial cell proliferation and angiogenesis, are also regulators of inflammatory cell infiltration [17]. Thus, it becomes clear that it is necessary to modulate both inflammation and angiogenesis when considering the FBR. However, given the nature of their relationship, a temporal aspect must be considered. That is, that initial reduction of the inflammatory response should be followed by an increase in the formation of blood vessels.

Multi-modal biomaterial delivery systems can facilitate the delivery of therapeutics in a temporally controlled manner [18]. Typical strategies involve combining scaffolds or hydrogels with microspheres to create systems that can temporally control therapeutic release. A type I collagen hydrogel system with type I collagen microspheres embedded within it can allow for the temporal delivery of nucleic acids, and has been shown *in vitro* using IL-10 pDNA and eNOS pDNA [19]. Using a composite microsphere-in-hydrogel system and differentially loading nucleic acids, the release of two separate doses of nucleic acids can be engineered. In the context of this study, the delivery of interleukin-6 (IL-6) targeting siRNA has been chosen as an anti-inflammatory agent. IL-6 is a key pro-inflammatory cytokine involved in the inflammatory cascade and infiltration of inflammatory cells [20,21]. IL-6 in particular plays a role in the recruitment of monocytes and neutrophils, and the differentiation of monocytes into macrophages [22]. Meanwhile, eNOS pDNA has been chosen as a pro-angiogenic factor, and has previously demonstrated its use in the context of biomaterial-mediated angiogenesis. Endothelial nitric oxide synthase (eNOS) is a pro-angiogenic enzyme that acts as a catalyst in the reaction of L-arginine to L-citrulline, resulting in the formation of nitric oxide (NO) [23]. NO promotes relaxation of blood vessels and the mobilization of endothelial progenitor cells (EPCs), an important step in the formation of new blood vessels [24,25]. In addition, NO has been shown to reduce IL-6 expression at high doses, in an NF- $\kappa$ B dependent pathway [26]. In contrast, at lower concentrations, NO has a stimulatory effect on NF- $\kappa$ B, exerting a pro-inflammatory effect. Thus, an siRNA-targeting IL-6 is released from within the hydrogel, while the release of eNOS pDNA is followed from the embedded microspheres. Through the delivery of IL-6 siRNA, the inflammatory response will be reduced, while eNOS pDNA will promote the formation of blood vessels. A subcutaneous rat model is used to test the efficacy of nucleic acid delivery to modify the balance between inflammation and angiogenesis during the FBR.

The ECM is a complex network of fibrillar and matricellular proteins, proteoglycans (PGs) and glycosaminoglycans (GAGs) that provides both structural and biochemical support to the cells

within [27]. It is well accepted that the local microenvironment, and specifically the ECM, plays a major role in the regulation of cell behaviour and function [28]. This is particularly apparent in cancer research where the ECM is dynamically involved in tumor progression, through increased immune evasion and angiogenesis in the microenvironment [29,30]. Thus, a means to examine changes in the ECM following modification of the FBR will prove useful. With this in mind, Raman microspectroscopy has been identified as a tool to reveal alterations in ECM following modification of the FBR. Raman microspectroscopy is gaining increased prominence in biomedical research as a label- and contact-free method to detect changes in the ECM. It has been used to distinguish between healthy and diseased tissue models *in vitro* [31], as well as detecting changes in ECM constituents [32]. Raman microspectroscopy generates a molecular fingerprint of the tissue, which can then be used to detect the presence of specific ECM components and their relative abundancies. Thus, by comparing between samples, changes in the ECM can be uncovered.

More recently, GAGs, and sulfated GAGs (sGAGs) in particular, have been identified as key components of the ECM that can dictate inflammatory responses and angiogenesis through interactions with cytokines and growth factors [33–35]. Specifically, changes in sulfated glycosaminoglycans (sGAGs) have been explored as a means by which the ECM controls the angiogenic potential of tissues [36]. Thus, modification of the inflammatory component of the FBR to an implanted biomaterial, as well as an increase in angiogenesis will result in changes in the local ECM microenvironment. This can manifest itself in terms of either the content of sGAGs or the growth factor binding activity of sGAGs. Through these changes, the ECM, and specifically the sGAGs, can dictate the response of the tissue by alteration of the microenvironment.

Thus, the hypothesis of this study is that delivery of optimal doses of IL-6 siRNA and eNOS pDNA through a collagen microsphere-in-hydrogel system will modulate the inflammatory response associated with the FBR and promote angiogenesis in a subcutaneous rat model. Furthermore, therapeutic nucleic acid delivery will effect changes in the ECM composition of the tissue, as measured by Raman microspectroscopy. The alteration in inflammation and angiogenesis in the tissue will lead to changes in the sGAG content and binding of sGAG to growth factors, specifically VEGF<sub>165</sub> and basic fibroblast growth factor (bFGF).

## 2. Materials and methods

### 2.1. Extraction of collagen

Type 1 atelocollagen was isolated as previously described [37]. Briefly, bovine tendons were blended, washed in buffer and suspended in 0.5 M acetic acid. The resulting solution was then pepsin treated and filtered to remove insoluble collagen telopeptides. The soluble collagen was then purified by repeated salt precipitation and centrifugation, followed by dialysis against 0.01 M acetic acid.

### 2.2. Fabrication of collagen microspheres

Hollow collagen microspheres were fabricated using the template method as previously described [38]. Briefly, commercially available polystyrene beads (Gentaur, Chicago, Illinois) of a defined size (1  $\mu$ m), were sulfonated to impart a negative charge. Following sulfonation, beads were resuspended in 0.5 M acetic acid. A collagen solution of 5 mg/ml was added to the beads at a weight ratio of 1:4 (collagen: beads). The resultant mixture was then stirred for four hours at room temperature. Crosslinking of the collagen coating was performed using pentaerythritol poly(ethylene glycol) ether tetrasuccinimidyl glutarate (4S-PEG), with

the active ester groups reacting with the free amino groups of collagen at a ratio of 1:4 (4S-PEG:free amino groups in the collagen). The mixture was agitated for two hours at room temperature. To produce a hollow sphere, the suspension of microspheres was diluted at a ratio of 1:1 with tetrahydrofuran (THF) and agitated for one hour. This washing step was repeated twice to ensure complete removal of polystyrene. Hollow spheres were then washed twice with ethanol and twice with water to ensure removal of any remaining THF.

### 2.3. Formation of polyplexes

The eNOS gene sequence, encoded into a pcDNA3 vector containing the CMV promoter, was kindly donated by Dr. Karl McCullagh (Regenerative Medicine Institute, National University of Ireland, Galway). Rat IL-6 siRNA (SMART pool: ON-TARGET plus IL-6 siRNA) was purchased from Thermo Scientific Dharmacon (Chicago, IL). Polyplexes were prepared by incubating the eNOS pDNA with a partially degraded polyamidoamine dendrimer (dPAMAM, Superfect™, Qiagen, Crawley, UK) (SF), as per the manufacturers instructions. The weight ratio of the dPAMAM to eNOS pDNA used was 9:1.

### 2.4. Loading of microsphere reservoirs with polyplexes

Collagen hollow microspheres of 1  $\mu\text{m}$  size were loaded with eNOS pDNA dPAMAM complexes, as previously described [38]. Briefly, collagen microspheres were suspended in phosphate buffered saline (PBS). Complexes of eNOS pDNA and dPAMAM were added to the microspheres, suspended in PBS, and agitated on a mechanical shaker for four hours at room temperature. Microspheres were spun down, and the supernatant was removed.

### 2.5. Dual-release collagen scaffold fabrication

A dual release system was fabricated by combining hollow collagen microspheres with a collagen hydrogel (Fig. 1). Microspheres 1  $\mu\text{m}$  in size were loaded with eNOS pDNA polyplexes mixed and re-suspended in a neutralized collagen/4S-PEG crosslinker solution containing IL-6 siRNA prior to gelation. The neutralized collagen solution with crosslinker containing nucleic acids was kept on ice and loaded into a syringe prior to delivery and gelation.

### 2.6. Characterisation of collagen system release profile

The release profile of Cy3 labelled siRNA and pDNA was characterized in PBS at 37 °C. eNOS Polyplex-loaded microspheres were re-suspended in a neutralized collagen/4S-PEG crosslinker solution containing a labelled IL-6 siRNA, prior to gelation. The combination of loaded-microspheres and 250  $\mu\text{l}$  of siRNA-containing gel-forming solution was pipetted into 24-well plate, and allowed to gel. After 15 min, 250  $\mu\text{l}$  of PBS was added to the gels. The supernatant was replaced at each timepoint. The collected supernatant was frozen until it was assayed for polyplex content by measuring fluorescence with a Varioskan Flash spectral scanning plate reader (Thermo Scientific, Vantaa, Finland).

### 2.7. In vivo implantation

All animal procedures and treatments were approved by the ethics committee at the National University of Ireland, Galway. In addition, animal care and management followed the Standard Operating Procedures of the Animal Facility at the National Centre for Biomedical Engineering Science, National University of Ireland, Galway. Animals were allowed to acclimatize for at least seven days

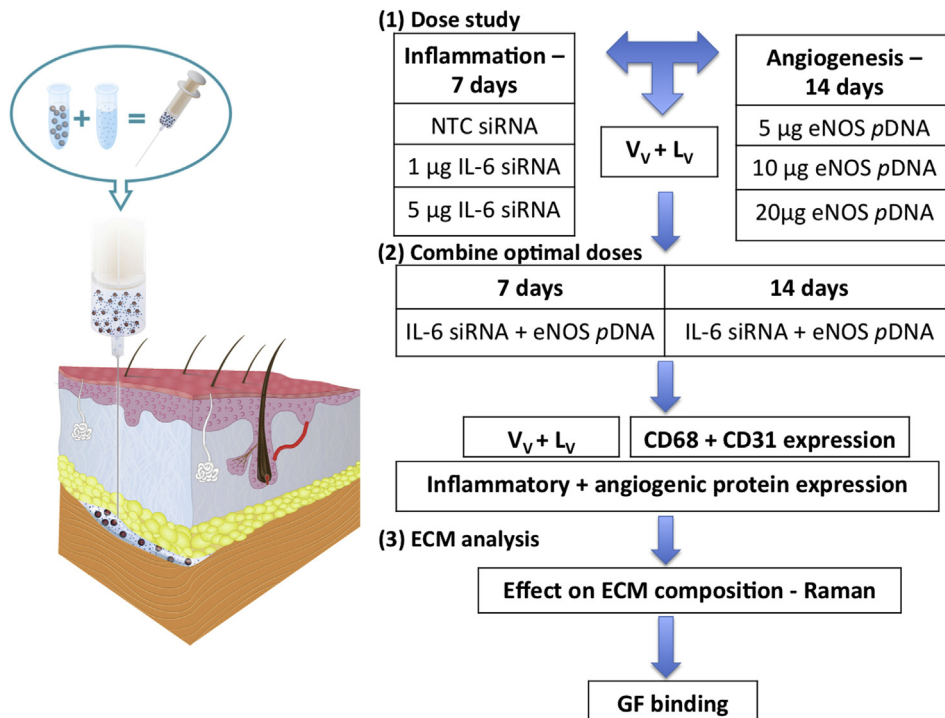


**Fig. 1.** Study design. Schematic illustrating the assembly and application of the collagen sphere-in-hydrogel system in the subcutaneous space, and the workflow of the study, from dose optimization (1) to combining the optimal dose (2) and analysis on the effect of the treatments on the composition of the ECM (3). ( $V_v$ : volume fraction of inflammatory cells,  $L_v$ : length density of blood vessels).

prior to any surgical procedures.

Female Lewis rats were anaesthetized by isoflurane inhalation (5% induction reducing to 1–2% for maintenance during procedures). The dorsum of rats was shaved and swabbed with iodine to minimize the risk of bacterial contamination. Prior to gelation, the hydrogel solution was taken into a syringe and injected into the subcutaneous space. Four injections were performed per animal, with a minimal spacing of 1 cm between each, and locations of samples were randomized.

#### 2.8. *In vivo* IL-6 siRNA dose optimization study

Two doses of IL-6 siRNA were tested in a collagen microsphere-in-hydrogel system. Either 1 or 5  $\mu\text{g}$  siRNA was suspended within a neutralized collagen solution containing 4S-PEG as crosslinker. These doses were selected as they are in the range of previous *in vivo* studies delivering interfering RNA [39]. A non-targeting control siRNA (NTC siRNA, Dharmacon, Chicago, IL) was delivered via the same collagen system, as a control to assess the tissue response to an siRNA-loaded collagen delivery system. For consistency, unloaded collagen microspheres were suspended within the pre-gelling solution prior to it being taken into a syringe and injected subcutaneously through a 29-G needle. Animals were sacrificed by  $\text{CO}_2$  asphyxiation at seven days and samples were removed and processed for analysis ( $n = 6$  per group).

#### 2.9. *In vivo* eNOS pDNA dose optimization study

Three doses of eNOS pDNA polyplexes were delivered from the collagen microsphere-in-hydrogel system. Either 5, 10 or 20  $\mu\text{g}$  of eNOS pDNA complexed with dPAMAM were loaded within 1  $\mu\text{m}$  collagen microspheres, and subsequently suspended within a neutralized collagen solution containing 4S-PEG as crosslinker. These doses were selected as they are in the range of previous studies delivering pDNA via collagen scaffolds [40]. In addition, it was decided not to use a significantly higher dose given concerns about possible vector-mediated toxicity at high doses. The collagen gel solution (prior to gelation occurring) was taken into a syringe and injected subcutaneously through a 29-G needle. Animals were sacrificed by  $\text{CO}_2$  asphyxiation at seven days and samples were removed and processed for analysis ( $n = 6$  per group).

#### 2.10. Combination of IL-6 siRNA and eNOS pDNA optimal doses

The optimal doses of IL-6 siRNA and eNOS pDNA (identified from the optimization studies) were combined and co-delivered using the collagen microsphere-in-hydrogel system. The optimal dose of IL-6 siRNA (1  $\mu\text{g}$ ) was loaded directly within the hydrogel phase while the optimal dose of eNOS pDNA polyplexes (10  $\mu\text{g}$ ) were loaded within the collagen microsphere phase and suspended within the collagen hydrogel pre-gelling solution. The combined system was injected subcutaneously through a 29-gauge needle. Animals were sacrificed by  $\text{CO}_2$  asphyxiation and samples were removed at 7 and 14 days and processed for analysis ( $n = 6$  per group).

#### 2.11. Tissue preservation and cryosectioning

Animals were sacrificed by  $\text{CO}_2$  asphyxiation and the tissue immediately excised. The explants were halved: one half was preserved for histological staining and immunostaining (10% buffered formalin for 24 h), and the other half for protein and sGAG analysis (immediately frozen in  $-80^\circ\text{C}$ ).

The tissue was cryoprotected by treatment with 30% sucrose for 24 h, followed by embedding and freezing in optimal cutting

temperature (OCT) medium. The tissue was then sectioned into 5  $\mu\text{m}$  thick sections. Serial sectioning was performed at four depths, a distance of 200  $\mu\text{m}$  apart.

#### 2.12. Histological staining

Standard hematoxylin and eosin (H&E) staining was performed on one section at each tissue depth. After staining, sections were dehydrated in increasing concentrations of ethanol, cleared in xylene and mounted using DPX mounting media.

#### 2.13. Stereology

Three images of each H&E stained section were taken at a magnification of  $40\times$  and used to quantify inflammation and angiogenesis stereologically using previously established protocols [41].

##### 2.13.1. Inflammation

**2.13.1.1. Volume fraction of inflammatory cells.** The volume fraction of inflammatory cells ( $V_V$ ) was used to quantify the inflammatory response. A 192-point grid was overlaid on  $40\times$  images of H&E stained tissue. The number of macrophage and neutrophil nuclei intersecting points of the grid is counted ( $P_P$ ), along with the total number of points on the tissue ( $P_T$ ). The volume fraction of inflammatory cells ( $V_V$ ) is calculated using the formula defined below:

$$V_V = P_P/P_T$$

##### 2.13.2. Angiogenesis

Angiogenesis was quantified using three different parameters: surface density ( $S_V$ ), length density ( $L_V$ ) and radial diffusion ( $R_{DIFF}$ ).

**2.13.2.1. Surface density ( $S_V$ ).** Images were overlaid with a cycloid grid of radius 40  $\mu\text{m}$  such that the grid was perpendicular to the skin epithelium. The total number of intersections between blood vessels and the test line ( $I$ ) was counted and the total length of test line ( $L_T$ ) calculated. The following formula was used:

$$S_V = 2 \times I/L_T$$

**2.13.2.2. Length density ( $L_V$ ).** Images were rotated  $90^\circ$  and a cycloid grid of radius 40  $\mu\text{m}$  applied. The total number of intersections between blood vessels and the test line ( $I$ ) was counted and the total length of test line ( $L_T$ ) calculated. The following formula was used:

$$L_V = 2 \times I/(L_T \times T_s)$$

where  $T_s$  is the thickness of the section.

**2.13.2.3. Radial diffusion ( $R_{DIFF}$ ).** The distance between blood vessels, termed radial diffusion, was calculated using the following formula:

$$R_{DIFF} = 1/\sqrt{(\pi \times L_V)}$$

#### 2.14. Immunofluorescence staining

Macrophages and blood vessels were identified by staining with anti-CD68, a pan-macrophage marker (1:300; ab125212, Abcam,

Cambridge, UK), and anti-CD31 (1:30; ab28364, Abcam, Cambridge, UK). Heat-mediated antigen retrieval was performed in a pressure-cooker in the appropriate buffers as previously described [42]. A secondary FITC-conjugated goat anti-rabbit IgG (1:250; A-11037, Life Technologies, Darmstadt, Germany) was used. Cell nuclei were stained with DAPI.

### 2.15. Protein extraction

Tissue samples were frozen at  $-80^{\circ}\text{C}$  immediately after extraction until analysis. Samples were thawed slowly on ice, chopped into small pieces and incubated in a lysis buffer containing a cocktail of protease inhibitors for five minutes. Samples were then mechanically disrupted in a bead mill homogeniser (TissueLyserLT, Qiagen, Hilden Germany) for five minutes at least three times until the tissue was completely homogenised and centrifuged at 15,000 g for 15 min. The protein fraction of the centrifuged sample was then extracted, aliquoted and stored at  $-80^{\circ}\text{C}$  until further use.

### 2.16. Protein analysis

The protein concentration of the extracted samples was determined using the bicinchoninic acid (BCA) assay (Thermo Scientific, Waltham, MA) and probed for 90 proteins simultaneously using a biotin label-based rat antibody array (RayBio<sup>®</sup>, Norcross, GA, USA) according to the manufacturer's instructions. Briefly, samples were pooled according to the treatment group to a total of 1 mg/ml and dialysed overnight to remove remaining lysis buffer and the protein membranes were blocked using a blocking buffer provided by the manufacturers. The proteins were labelled with biotin and incubated with the antibody labelled membranes overnight at  $4^{\circ}\text{C}$ . HRP-conjugated streptavidin was reacted with the membranes and afterwards treated with the incubation buffer provided. Membranes were exposed using a Kodak<sup>™</sup> Image Station 4000 MM Pro (Kodak, Japan). Micrographs of the exposed membranes were digitally evaluated using ImageJ. The images obtained were imported into ImageJ and analysed using a protein array analyser plug-in by normalising to the given positive control signals on the membranes. Samples were analysed and normalised to the unloaded collagen system-treated controls.

### 2.17. Raman analyses of the host response to sphere-in-hydrogel implant

Tissue sections (thickness, 30  $\mu\text{m}$ ) were analysed via Raman microspectroscopy. A custom-built Raman microspectroscopy system was used for all measurements as previously described [43,44]. All measurements were performed using a 60 $\times$  water immersion objective (NA 1.2, Olympus). Using an automated stage, 100 spectra were taken at 100 points throughout the tissue. An acquisition time of 100 s with 85 mW laser power were used for each spectrum. Raman spectra were acquired in the wavenumber range of 0–2000  $\text{cm}^{-1}$ . Raman spectra were recorded using the Andor software package (Andor iDus, Belfast, Northern Ireland). All measurements were performed from specimens on glass slides. The glass background signal was subtracted from the sample signal using the OPUS<sup>®</sup> software 4.2 (Bruker Optik GmbH, Ettlingen, Germany). Additionally, OPUS<sup>®</sup> software 4.2 was used to cut the Raman spectra into the spectral 400–1800  $\text{cm}^{-1}$  region and baseline correction performed.

### 2.18. Principal component analysis (PCA)

PCA is a multivariate method utilized to analyse the variances in a spectral dataset. PCA is valuable to identify significant shifts in the

spectra between sample groups. Prior to the PCA computation, all Raman spectra were imported to the UnscramblerX<sup>®</sup> 10.2 Software (CAMO, Oslo, Norway). PCA was performed on vector-normalized Raman spectra with a pre-defined list of Raman shift wavelengths primarily associated with GAGs, PGs and other ECM components. Principal components (PCs) were calculated using the non-linear iterative partial squares (NIPALS) algorithm. As a result of the PCA, every spectrum is described by score values. Separation of score plots reveal differences between sample groups, while loadings indicate the region of the spectra where the primary differences occur.

### 2.19. sGAG extraction

Extraction of total sGAGs was performed as previously described [36]. Briefly, tissue samples were digested in an extraction buffer (50 mM Tris, 10  $\mu\text{M}$  NaCl, 3  $\mu\text{M}$   $\text{MgCl}_2$ , 1% Triton-x100, pH 7.9) using proteinase K (200  $\mu\text{g}/\text{ml}$ ) and DNase (10 U per 25  $\mu\text{g}$  of tissue sample), followed by NaCl addition to a final 2 M NaCl concentration. Samples were then vigorously agitated for ten minutes and the remaining proteins and peptides were precipitated by adding TCA (final 10%). Supernatants were cleared by chloroform, followed by dialysis of the aqueous phase (Pierce, Slide-A-Lyzer Mini Dialysis Units 3500 molecular weight cut-off) against the extraction buffer and then pure water. After freeze-drying, extracted sGAGs were dissolved in water.

### 2.20. Heparin/sGAG binding competition assay towards growth factors

ELISA plates were coated overnight at  $4^{\circ}\text{C}$  with a 2  $\mu\text{g}/\text{ml}$  BSA-heparin conjugate solution prepared, as previously described [45]. After washing the plates with 0.05% PBS-Tween 20, the wells were saturated with 3% PBS-BSA for one hour at room temperature. A set amount of the growth factor (VEGF<sub>165</sub> and bFGF) to be studied was added to the plate. Working growth factor concentrations were fixed at 30 ng/ml for VEGF<sub>165</sub> and 6.25 ng/ml of bFGF, having been previously optimized. These concentrations were used to determine the capacity of competing soluble extracted GAGs to inhibit binding of the growth factor to the immobilized heparin. Growth factors and extracted GAGs were simultaneously added to the wells. After one hour of incubation at room temperature, wells were washed, and the growth factor remaining bound to heparin was detected by incubation with the corresponding primary antibody followed by a peroxidase-labelled secondary antibody. Peroxidase activity was detected by a peroxidase activity detection kit using the 3,3',5,5'-tetramethylbenzidine substrate, following the manufacturers indications. Heparin was used as a positive control of growth factor binding.

### 2.21. Statistical analysis

GraphPad Prism<sup>®</sup> (v.5 GraphPad Software, San Diego, CA, USA) was used for all statistical analyses. Analysis of variance (ANOVA) was used followed by Tukey's post-hoc test to determine statistical significance between groups. All graphical data is presented as mean  $\pm$  standard deviation. p values of  $<0.05$  were considered statistically significant.

## 3. Results

### 3.1. Collagen system characterisation of release *in vitro*

The nucleic acid release profile from the collagen system was characterized *in vitro* using fluorescence-labelled pDNA. Fig. 2

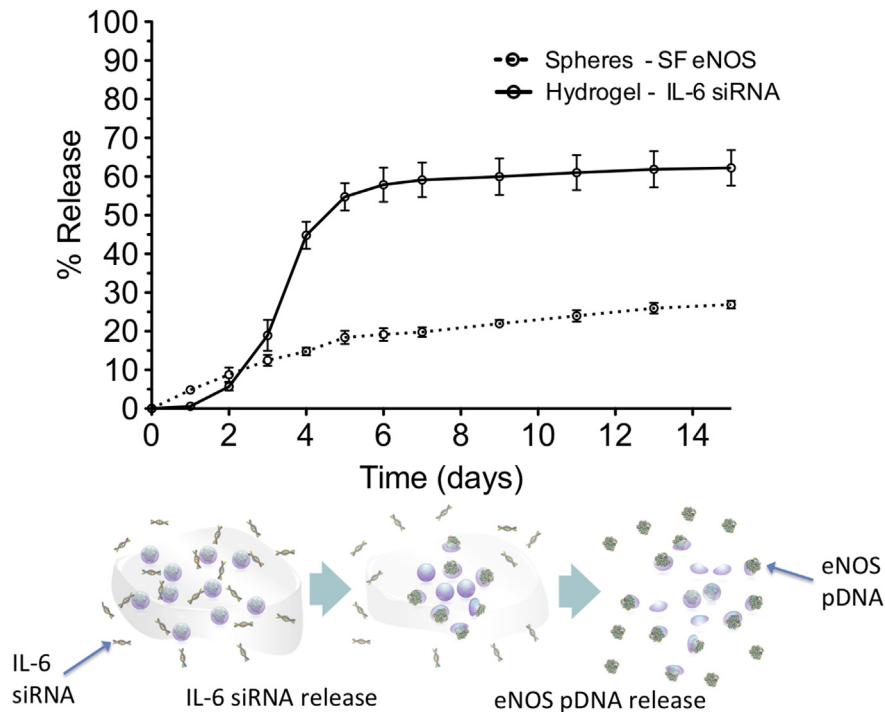


**Fig. 2.** Multi-modal collagen gene reservoir. The release profile of siRNA is much quicker than the release profile of pDNA, which can be attributed to the design of the system with siRNA within the hydrogel and pDNA within the microspheres, as depicted in the schematic. Data represents mean  $\pm$  SD ( $n = 3$ ).

reveals a differential release of siRNA and pDNA loaded within the collagen hydrogel and the collagen microspheres, respectively. By day three, approximately 20% of the siRNA was released from the system, while about 10% of the pDNA was released. By five days, over 50% of the siRNA was released; while in contrast less than 20% of the pDNA was released (Fig. 2). This indicates a delayed release of nucleic acids from the microsphere phase of the system compared with release from the hydrogel phase of the system.

### 3.2. IL-6 siRNA dose optimisation - inflammation

Delivery of IL-6 targeting siRNA was analysed *in vivo* following biomaterial implantation. The incorporated collagen sphere-in-hydrogel system was implanted subcutaneously and removed after seven days. Two doses of IL-6 siRNA were examined (1 and 5  $\mu\text{g}$ ) along with a non-targeting control siRNA (NTC siRNA). Delivery of NTC siRNA was used as a baseline to assess the tissue response to the delivered IL-6 siRNA. The seven-day time point was chosen as an early time point to assess the inflammatory response following implantation of the foreign material. The *in vivo* infiltration of inflammatory cells (primarily neutrophils and macrophages) in response to the system described in this paper was evaluated by the analysis of H&E sections. It was observed that treatment with 1 and 5  $\mu\text{g}$  of IL-6 siRNA resulted in a reduction in the volume fraction of inflammatory cells (52% and 42% respectively), compared with the NTC siRNA, as shown in Fig. 3B. No effect was observed in terms of changes in the surface density of blood vessels as a result of IL-6 siRNA at either dose (Fig. 3A). Thus, incorporation of IL-6 siRNA within the collagen delivery system resulted in a significant reduction in the volume fraction of inflammatory cells with non-significant effect in angiogenesis.

### 3.3. eNOS pDNA optimisation – angiogenesis

The capacity of subcutaneously implanted eNOS pDNA and

control biomaterials to promote angiogenesis was analysed. As shown in Fig. 4, delivering 5  $\mu\text{g}$  eNOS pDNA resulted in almost doubling of the surface density of blood vessels ( $8.6 \text{ mm}^{-1}$  compared with  $4.7 \text{ mm}^{-1}$ ). The medium dose, 10  $\mu\text{g}$  eNOS pDNA, showed a further increase in the length density of blood vessels with an almost three-fold increase observed over that of the control ( $12.9 \text{ mm}^{-1}$ ). The 10  $\mu\text{g}$  eNOS pDNA dose resulted in greater surface density of blood vessels than that of both the unloaded collagen sphere-in-hydrogel system, but also the system loaded with 5  $\mu\text{g}$  eNOS pDNA. No change was observed in the length density between the 10  $\mu\text{g}$  and 20  $\mu\text{g}$  treated groups ( $12.9 \text{ mm}^{-1}$  and  $13.2 \text{ mm}^{-1}$ , respectively), suggesting a peak in the dose response (Fig. 4).

Analysis of the volume fraction of inflammatory cells revealed a reduction in inflammation with the 10  $\mu\text{g}$  eNOS pDNA group (43% reduction) compared with the unloaded collagen sphere-in-hydrogel system. No significant changes were detected between the other treatment groups, 5  $\mu\text{g}$  and 10  $\mu\text{g}$  eNOS pDNA, in terms of changes in volume fraction of inflammatory cells. Considering the increase in length density of blood vessels and the reduction in volume fraction of inflammatory cells, the 10  $\mu\text{g}$  eNOS pDNA treated group was identified as the optimal dosing regimen of eNOS pDNA from the collagen sphere-in-hydrogel system. These results indicate that delivering eNOS pDNA results in a significant increase in surface density of blood vessels and a reduction in the volume fraction of inflammatory cells.

### 3.4. Combination of IL-6 siRNA and eNOS pDNA optimal doses

#### 3.4.1. Inflammation

Following on from the selection of the optimal doses of anti-inflammatory IL-6 siRNA (1  $\mu\text{g}$ ) and the pro-angiogenic eNOS pDNA (10  $\mu\text{g}$ ) to modify the tissue response to the implanted collagen sphere-in-hydrogel system, these two optimal doses were combined, co-delivered and the tissue response, in terms of

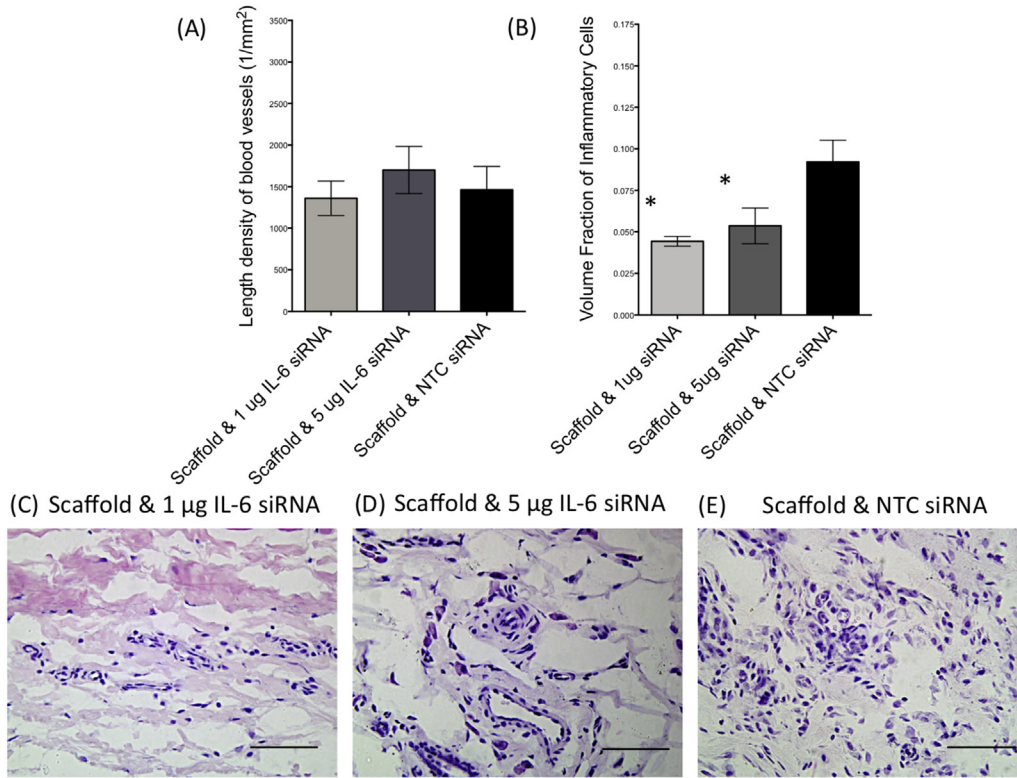


**Fig. 3.** Optimization of IL-6 siRNA dose. (A) No effect was observed on length density of blood vessels between groups. (B) Volume fraction of inflammatory cells was reduced following treatment with scaffold and IL-6 siRNA at doses of 1 and 5 µg compared with the scaffold loaded with non-targeting control (NTC) siRNA. Representative H&E stained sections of (C) NTC siRNA, (D) 1 µg IL-6 siRNA and (E) 5 µg IL-6 siRNA treated-groups, respectively. Data represents mean ± SD (n = 6). Analysis performed using one-way ANOVA, p < 0.05. \* denotes statistical significance versus scaffold & NTC siRNA group. Scale bars indicate 25 µm.

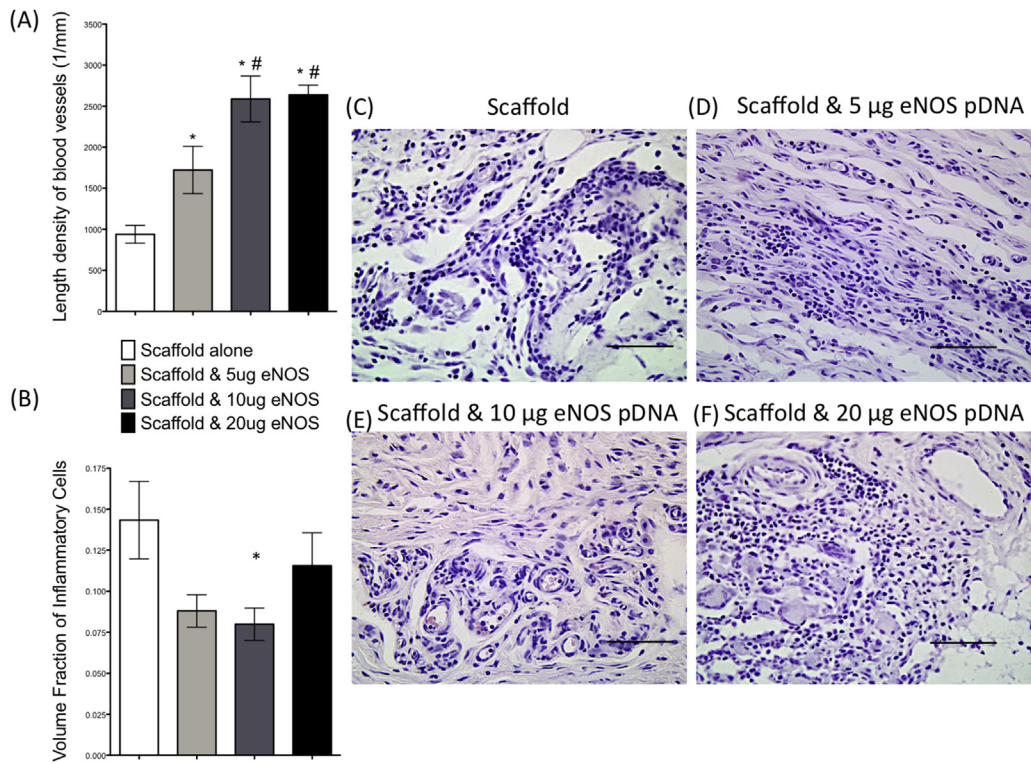


**Fig. 4.** Optimization of eNOS pDNA dose. (A) Length density of blood vessels was increased following treatment with eNOS pDNA at doses of 5 µg, 10 µg and 20 µg compared with the control scaffold alone. (B) No difference was observed in the volume fraction of inflammatory cells between groups, although amongst the eNOS pDNA treated-groups, a trend towards an increase in volume fraction in the 20 µg eNOS pDNA treated-group was observed. Representative H&E stained sections of (C) scaffold alone, (D) scaffold & 5 µg eNOS pDNA, (E) scaffold & 10 µg eNOS pDNA and (F) scaffold & 20 µg eNOS pDNA, respectively. Data represents mean ± SD (n = 6). Analysis performed using one-way ANOVA, p < 0.05. \* denotes statistical significance versus scaffold alone group. # denotes statistical significance versus 5 µg eNOS pDNA treated group. Scale bar indicates 25 µm.

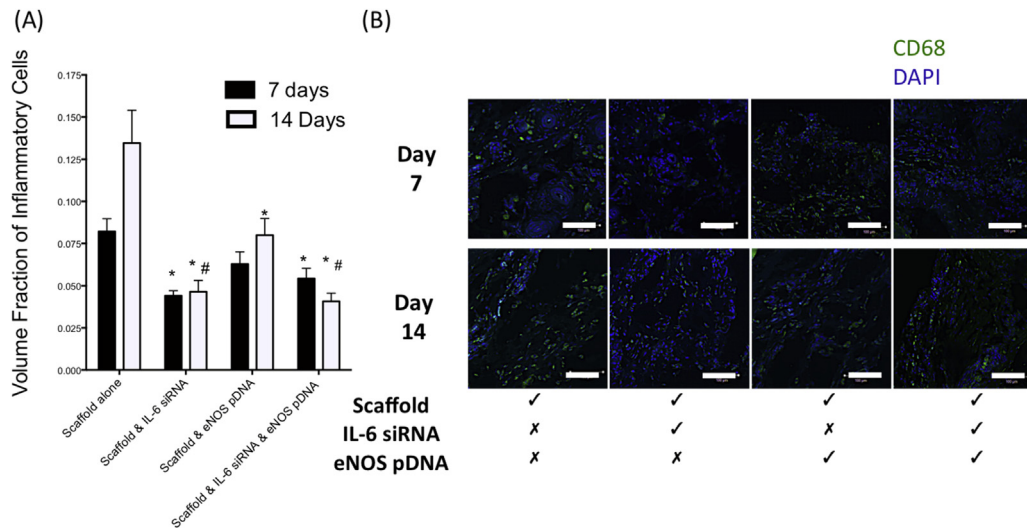


**Fig. 5.** Effect of dual delivery on inflammation. A reduced volume fraction of inflammatory cells was observed in groups treated with IL-6 siRNA, with or without eNOS pDNA at both 7 and 14 days. Representative images reveal a reduction in the presence of CD68+ cells in IL-6 siRNA treated groups, alone or in combination with eNOS pDNA. Data represents mean  $\pm$  SD (n = 6). Analysis performed using one-way ANOVA,  $p < 0.05$ . \* denotes statistical significance versus scaffold alone group at same timepoint. # denotes statistical significance versus eNOS pDNA treated group at 14 days. Scale bar indicates 100  $\mu$ m.

inflammatory response and angiogenesis, and examined at both 7 and 14 days. Combining IL-6 siRNA within the collagen hydrogel/microsphere system resulted in a reduction in the volume fraction of inflammatory cells. A reduction of 46% and 34% in volume fraction of inflammatory cells for delivery of IL-6 siRNA alone or IL-6 siRNA and eNOS pDNA was observed when compared with the unloaded collagen system alone at seven days (see Fig. 5). There was no significant change in the volume fraction of inflammatory cells in the eNOS pDNA treated group at seven days.

At 14 days a similar observation was made. Compared with the collagen delivery system alone there was a reduction in the volume fraction of inflammatory cells by 65% with the addition of IL-6 siRNA and 69% with delivery of IL-6 siRNA and eNOS pDNA. Delivery of eNOS pDNA alone via the collagen delivery system resulted in a reduction in volume fraction of inflammatory cells of 40% compared with the unloaded collagen delivery system.

To confirm differences in the relative presence of inflammatory cells between the various treatment groups, immunofluorescence staining was performed. Macrophages, a key cell in the inflammatory process, were stained with a CD68 antibody. Representative images are shown in Fig. 5B. It can be seen that there are less CD68-positive cells in the IL-6 siRNA treated group and the IL-6 siRNA and eNOS pDNA dual-treated group compared with the control group. In addition, there is a reduction in CD68-positive cells in the eNOS pDNA treated group, but this reduction is not as much as the groups in which IL-6 siRNA is delivered. This trend can be seen at both the 7 and 14 day time points.

#### 3.4.2. Angiogenesis

The effect of co-delivery of IL-6 siRNA and eNOS pDNA on vascularization of the host tissue was assessed via stereological analysis of H&E stained sections. At seven days there was a statistically significant increase in the length density of blood vessels in the eNOS pDNA treated group and the IL-6 siRNA and eNOS pDNA dual-treated group when compared with the unloaded collagen hydrogel/microsphere system (control group), with an almost two-fold increase observed (2617 and 3018  $\text{mm}^{-2}$ , respectively, compared with 1681  $\text{mm}^{-2}$ ), as seen in Fig. 6. There was no significant difference between the eNOS pDNA treated group and the IL-6 siRNA and eNOS pDNA dual-treated groups. The IL-6 siRNA

treated group showed no significant difference when compared with the control group. Further data on the perfusion of the tissue was acquired by measuring the radial diffusion distance, revealing the average distance between adjacent blood vessels. It was observed that eNOS pDNA treated groups, with or without IL-6 siRNA, had a significantly reduced radial diffusion distance compared with the control. The radial diffusion distance in the IL-6 siRNA treated group was not significantly different to the control.

A similar effect was observed at 14 days. Again, the length density of blood vessels was greatest in the eNOS pDNA treated groups, both without and with the addition of IL-6 siRNA (2568  $\text{mm}^{-2}$  and 2910  $\text{mm}^{-2}$ ). The length density of blood vessels in both of these groups was significantly greater than that of the control, with an almost three-fold increase observed (939  $\text{mm}^{-2}$ ). The IL-6 siRNA treated group was not statistically different to the control (1244  $\text{mm}^{-2}$ ). Radial diffusion distance was also statistically different between eNOS treated groups (compared with the control and IL-6 siRNA alone treatment). This suggests that co-delivering IL-6 siRNA and eNOS pDNA has an anti-inflammatory and pro-angiogenic effect.

To confirm the presence of blood vessels, immunofluorescence staining was performed for CD31, an endothelial cell marker. Representative images are shown in Fig. 6D. There is a greater presence of CD31-positive endothelial cells in both eNOS pDNA treated groups compared with either the control or the IL-6 siRNA treated groups. This effect is apparent at both 7 and 14 days.

#### 3.5. Protein expression

An antibody-membrane array was performed to analyse the expression of various inflammatory and angiogenic proteins following treatment. Results for each membrane were normalized to the control (unloaded collagen sphere-in-hydrogel treatment) tissue. The proteins that have shown differential expression (increased or decreased) are displayed graphically in Fig. 7, for 7 and 14 days. For clarity, proteins have been grouped in terms of whether they relate primarily to inflammation or angiogenesis, with proteins found downregulated in red (in the web version) and those found upregulated in blue (in the web version). Pooled samples from each group were analysed to determine the global

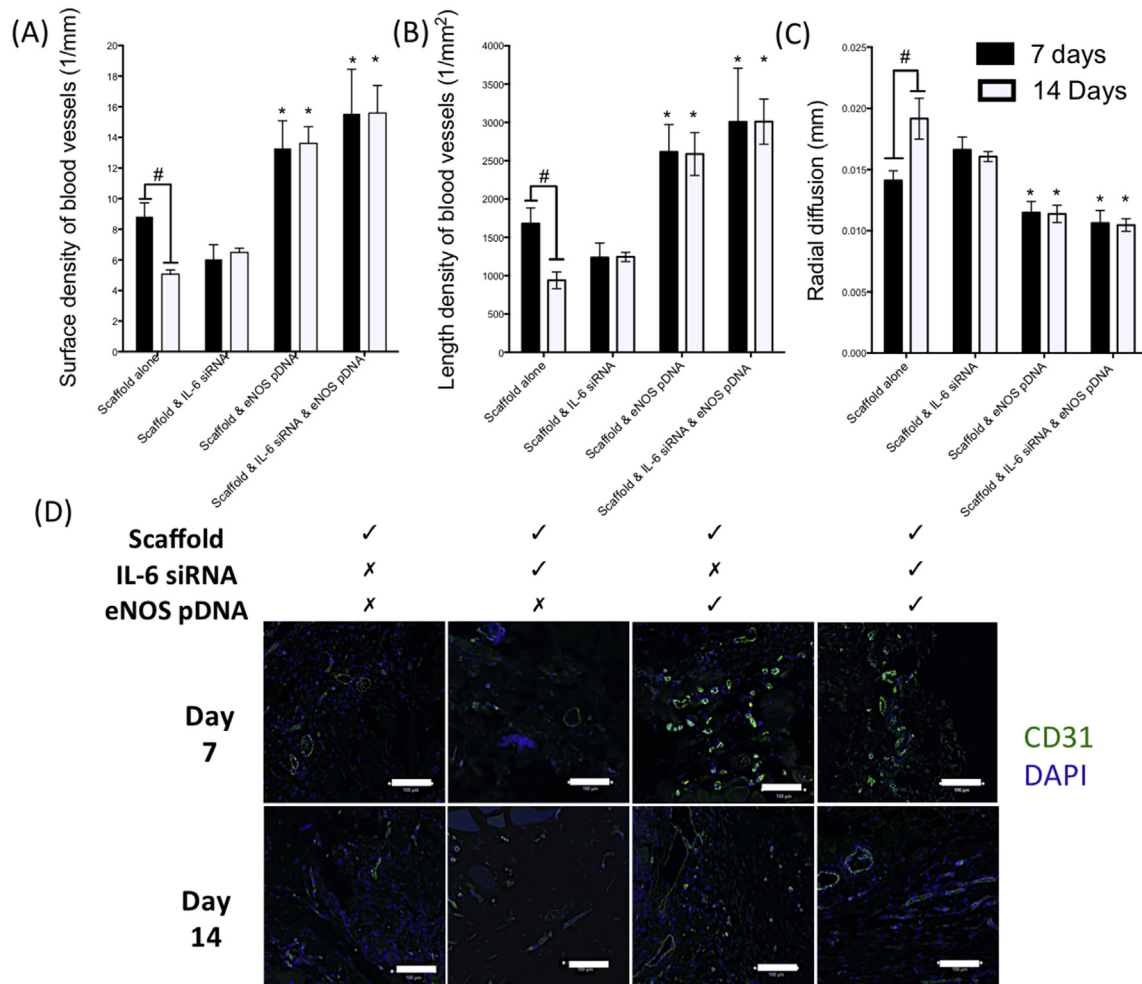


**Fig. 6.** Effect of dual delivery on angiogenesis. An increase in surface and length density of blood vessels was observed following treatment with eNOS pDNA, alone or in combination with IL-6 siRNA. Conversely, a reduction was observed in the radial diffusion distance following eNOS pDNA delivery, either alone or in combination with IL-6 siRNA. Representative images reveal an increase in CD31 + cells following eNOS pDNA delivery, with or without co-delivery of IL-6 siRNA. Data represents mean  $\pm$  SD ( $n = 6$ ). Analysis performed using one-way ANOVA,  $p < 0.05$ . \* denotes statistical significance versus scaffold alone group at same timepoint. # denotes statistical significance between groups. Scale bar indicates 100  $\mu$ m.

effect of the various treatment groups. Fig. 7A shows that the delivery of IL-6 siRNA resulted in a reduction in IL-6 protein expression at seven days. In addition, the expression of a range of inflammatory mediators including IL-1 $\alpha$  and TNF- $\alpha$ , as well as cytokine-induced neutrophil chemoattractant 2 and 3 (CINC-2/3), macrophage derived chemokine (MDC), macrophage inflammatory protein-2 (MIP-2), interferon-inducible protein-10 (IP-10) and granulocyte-macrophage colony-stimulating factor (GM-CSF). In addition to a reduction in inflammatory cytokines, decreased expression of bFGF, FGF-binding protein (FGF-bp), VEGF and VEGF-C, all angiogenic factors, was also detected. CXCR4, PDGF-AA, and Neuropilin-2 (NRP-2) were overexpressed.

Addition of eNOS pDNA to the collagen sphere-in-hydrogel system resulted in an increase in the expression of a number of angiogenic factors, amongst them bFGF, FGF-bp, CXCR4, PDGF-AA, VEGF and Neuropilin-2 (NRP-2). Conversely, an increase was observed in the expression of three inflammatory cytokines, CINC-2/3 and MIP-2.

The combination of IL-6 siRNA delivery and eNOS pDNA from the collagen sphere-in-hydrogel system resulted in a modulation of the expression of both inflammatory and angiogenic factors at seven days. As shown in Fig. 6A, there is both a reduction in IL-6,

TNF- $\alpha$  and GM-CSF. In addition, there was an increased expression of angiogenic factors, similar to that of the eNOS pDNA treated group with increased FGF-bp, CXCR4, PDGF-AA, VEGF, NRP-2 and MMP-8.

A similar observation was made at 14 days (Fig. 7B) as was made at 7 days with regard to protein expression. Delivery of IL-6 siRNA via the collagen sphere-in-hydrogel system reduced IL-6 protein expression, along with the expression of IP-10 and resistin-like molecule-beta (RELM- $\beta$ ). An increase in interleukin-4 (IL-4) and -13 (IL-13) was also observed. Increased expression of angiogenic factors (VEGF and VEGF-C) and receptors (NRP-2) was also seen.

At 14 days, delivery of eNOS pDNA resulted in an increase in a range of angiogenic factors similar to that observed at 7 days, with the exception of FGF and NRP-2, which were unchanged compared with the control. There was also an increase in osteopontin (OPN) and matrix metalloproteinase-8 (MMP-8) expression. Increased FADD expression was also observed, along with a reduction in IL-10 expression.

The combined delivery of IL-6 siRNA and eNOS pDNA through the collagen sphere-in-hydrogel system resulted in a number of substantial changes in protein expression. As with delivery of IL-6 siRNA alone, there was a reduction in IL-6 expression. An

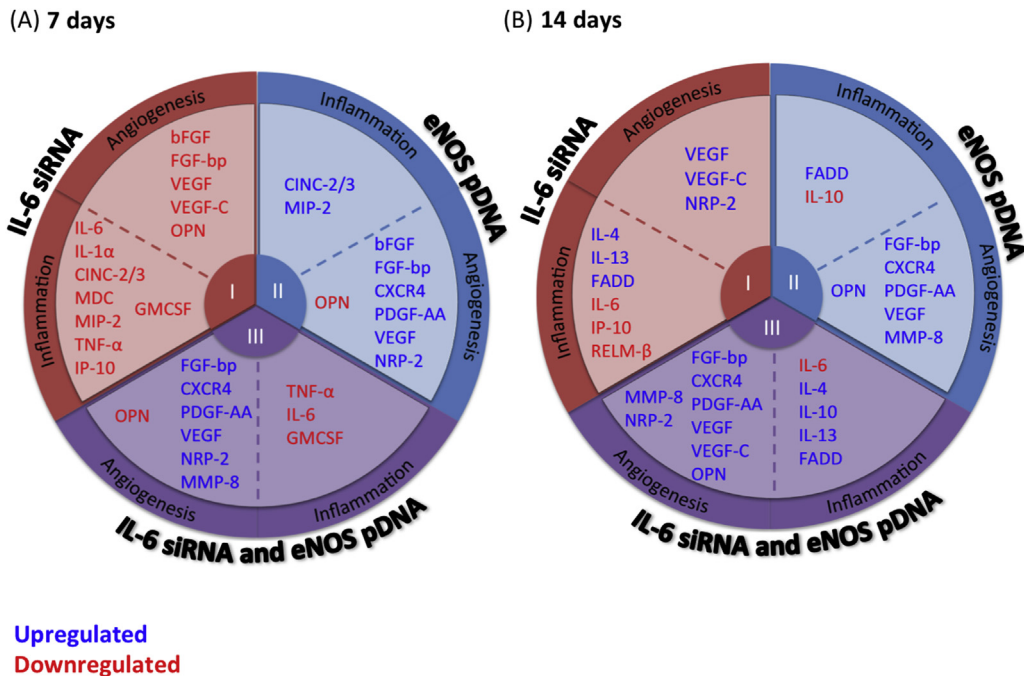


**Fig. 7.** Change in protein expression. Alterations in protein expression detected via protein blot array between the treatment groups and the control at 7 and 14 days. The proteins have been grouped in terms of proteins with functions primarily associated with inflammation or angiogenesis.

increased expression of IL-4, IL-10 and IL-13 was also observed. As with the eNOS pDNA group, there was also an increase in FADD, an anti-inflammatory mediator. In terms of angiogenic factors, FGF-bp, CXCR4, PDGF-AA, VEGF, VEGF-C, OPN, NRP-2 and MMP-8 are significantly upregulated, as would be expected with the increase observed in surface and length density of blood vessels.

### 3.6. Raman microspectroscopy

Raman microspectroscopy was performed in samples from all groups at both the 7 and 14 day time points following treatment with the collagen sphere-in-hydrogel system. Results revealed differences between the tissue ECM following treatment with the collagen sphere-in-hydrogel system. PCA analysis revealed a distinct separation between the control, unloaded sphere-in-hydrogel system and the IL-6 siRNA and eNOS pDNA loaded system at seven days (Supplementary Information). Analysis of the spectral intensity revealed changes at peaks 853, 882, 921 and 1065  $\text{cm}^{-1}$  when compared to the control (Fig. 8). These peaks are potentially associated with changes in the chondroitin sulfate proteoglycans and sulfation patterns, indicating changes in sGAG of the tissue.

### 3.7. Growth factor binding by sGAG extracted from tissue

Binding of VEGF<sub>165</sub> and bFGF by tissue-extracted sGAG was tested using a growth factor binding assay. At seven days, there was a significant increase in the binding of sGAG with both growth factors tested in eNOS pDNA treated groups (Fig. 9). For VEGF<sub>165</sub> binding, it is noticeable that there is a significant increase in sGAG binding at seven days in the eNOS pDNA treated samples (45.6% and 50.1% for eNOS pDNA groups without and with IL-6 siRNA, respectively) versus the control or IL-6 siRNA treated samples respectively, (31.5% and 22.2% for the control and IL-6 siRNA treated groups, respectively). Binding to bFGF shows a similar

effect, with an increase observed in the eNOS pDNA treated groups (42.6% and 51.5% without and with IL-6 siRNA, respectively) compared with the control (29.5%) and the IL-6 siRNA alone treated groups (23.6%).

By 14 days, the eNOS pDNA treated samples returned to baseline for bFGF binding (24.9% without and 22.5% IL-6 siRNA), with no difference observed between samples. Binding of VEGF<sub>165</sub> by sGAG was reduced to levels below that of the control (18% and 6% for eNOS pDNA and IL-6 siRNA and eNOS pDNA dual treatment respectively, compared with 24% for the control).

## 4. Discussion

Collagen microspheres and a collagen hydrogel were combined to form a dual release IL-6 siRNA and eNOS pDNA system. As size dictates uptake by cells, particularly macrophages [46,47], the size of microspheres used was an important consideration. Thus, 1  $\mu\text{m}$  collagen microspheres were chosen as previous studies by this group have shown that 1  $\mu\text{m}$  collagen microspheres were not internalized by activated and differentiated THP-1 cells [48]. Our results show that assembly of the collagen microsphere and hydrogel systems allowed for the temporal release of two distinct forms and doses of nucleic acids. This is shown in Fig. 2A, where the release profiles are photometrically characterized. Release of IL-6 siRNA from the hydrogel phase of the system was more rapid compared with the eNOS pDNA delivery from the microsphere phase. This emphasizes the possibility of a delayed release, with release from the hydrogel phase of the system more rapid compared with the microsphere phase of the system. Release from the hydrogel phase of the system was more rapid compared with the microsphere phase of the system. To clarify that the release profile is due to the difference in loading (in microspheres compared with in hydrogel) rather than the difference between siRNA and pDNA, the release of pDNA from the microsphere and hydrogel phases of the system was compared (Supplementary

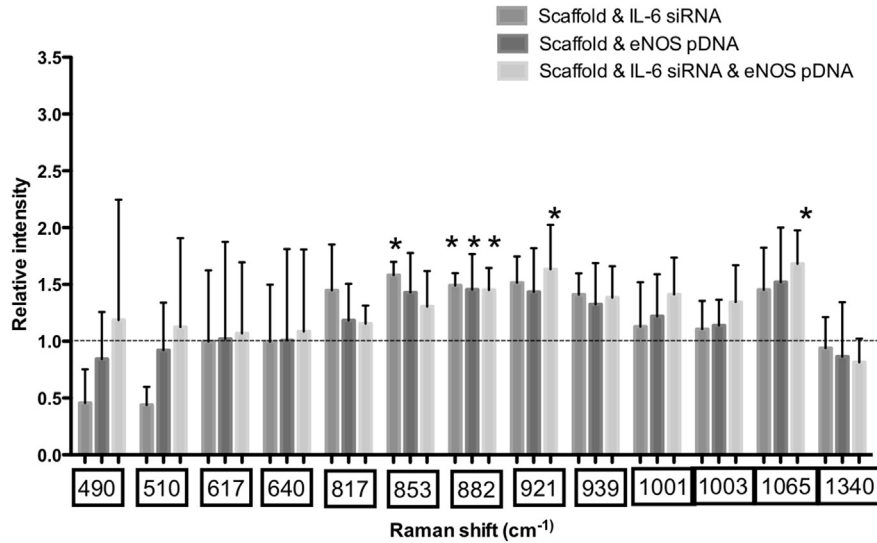


**Fig. 8.** Raman intensity analysis of selected ECM components at seven days. Analysis of the difference in intensity in specific peaks between groups. The intensity of the scaffold alone group is set at 1, and all other groups shown relative to this. Data represents mean  $\pm$  SD ( $n = 6$ ). Analysis performed using one-way ANOVA,  $p < 0.05$ . \* denotes statistical significance versus scaffold alone group.

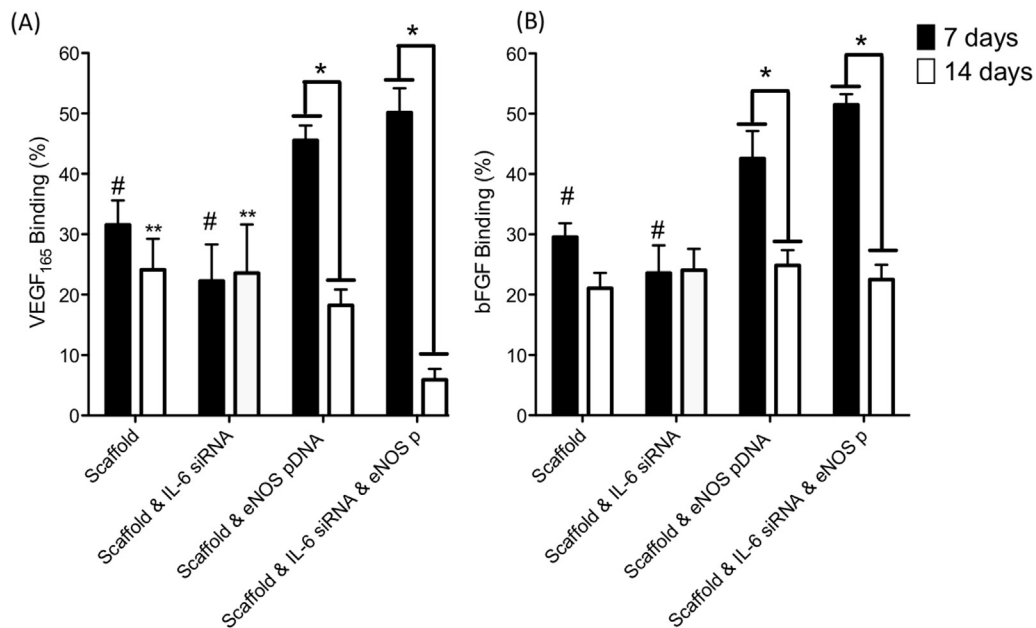


**Fig. 9.** Growth factor binding of sGAGs extracted from tissue samples changes with eNOS pDNA treatment. Treatment with eNOS pDNA increased the ability of sGAG extracted from the tissue to bind VEGF<sub>165</sub> and bFGF at 7 days, either alone or in combination with IL-6 siRNA treatment. Data represents mean  $\pm$  SD ( $n = 3$ , 2 pooled samples). Analysis performed using one-way ANOVA,  $p < 0.05$ . \* denotes statistical significance versus scaffold alone group at 7 days. \*\* denotes statistical significance compared with scaffold & IL-6 siRNA & eNOS pDNA group at 14 days. # denotes statistical significance compared with scaffold & eNOS pDNA and scaffold & IL-6 siRNA & eNOS pDNA groups at 7 days.

**Information).** It was observed that there was a clear difference between the release profiles of pDNA loaded within microsphere compared with directly loading in the hydrogel.

The inflammatory response is a key factor that determines the success or failure of a biomaterial implant [49]. Excessive inflammation results in the rejection of a biomaterial, which may then be degraded or encapsulated within a fibrotic capsule, essentially allowing the body to spatially exclude the implant. IL-6 is a pro-inflammatory cytokine produced by fibroblasts as well as inflammatory cells [50,51], and is involved in the progression of inflammation and the foreign body reaction [7]. Thus, the delivery of IL-6 targeting siRNA was proposed as an approach to reduce the

inflammatory response. Two doses of IL-6 siRNA were examined (1 and 5  $\mu$ g), along with NTC siRNA.

Stereological examination of H&E stained tissue sections revealed that incorporation of IL-6 siRNA within the collagen delivery system significantly reduced the volume fraction of inflammatory cells present. The volume fraction of inflammatory cells following delivery of NTC siRNA can be considered the 'standard inflammatory response' to an RNA-loaded collagen delivery system. Thus, the reduction observed in infiltrating inflammatory cells (primarily neutrophils and macrophages) compared to NTC siRNA can be directly attributed to the IL-6 targeting siRNA. Importantly, the delivery of an IL-6 targeting siRNA did not significantly affect

angiogenesis in the tissue. While IL-6 is primarily associated with inflammation, it is also linked with angiogenic processes both in disease and development [52,53]. However, here it was observed that delivery of an IL-6 targeting siRNA does not significantly impact the surface density of blood vessels at seven days when compared to delivery of a NTC siRNA (Fig. 3). With no difference observed in volume fraction of inflammatory cells between 1 and 5  $\mu\text{g}$  IL-6 siRNA doses, the lower 1  $\mu\text{g}$  dose was deemed sufficient to modify the inflammatory response to the implanted collagen sphere-in-hydrogel system.

One of the primary causes of the failure of implanted biomaterials is the failure of vascularization of the implant. Delivery of angiogenic signals such as growth factors is one avenue that has been explored. However, issues such as the short *in vivo* half-life have reduced the effectiveness of this approach [54]. Nucleic acid delivery offers an opportunity to bypass this issue by providing a continuous supply of pro-angiogenic signals. Delivery of an eNOS encoding plasmid via biomaterial systems has previously been shown to increase vascularization in a diabetic wound model [55,56]. The 14 day time point in this study was chosen as an appropriate time to observe blood vessel formation for a number of reasons. The first of which is due to the release profile of the eNOS polyplexes from the microsphere phase of the sphere-in-hydrogel system *in vitro*, which is more delayed compared with the release from the hydrogel portion. In addition, following implantation, a tissue response exists, usually involving a short-term increase in blood vessel formation. In order to differentiate between blood vessels formed due to the foreign body response following the implantation procedure and those due to the delivery of the eNOS gene itself, 14 days was chosen as an appropriate time point. Previous efforts aimed at the delivery of the eNOS gene have utilized various vectors, including lipoplexes and viral vectors [55,56]. In this project, a dPAMAM transfection reagent was used as a vector. In all cases, the efficiency of delivery and transfection is dependent on the vector used, thus dose optimization is required. Three doses of eNOS pDNA, all complexed with dPAMAM, were explored: low, medium and high (5  $\mu\text{g}$ , 10  $\mu\text{g}$  and 20  $\mu\text{g}$ , respectively). Stereological examination found that delivery of the lowest dose of eNOS pDNA resulted in a statistically significant increase in the surface density of blood vessels compared with a collagen sphere-in-hydrogel system without loaded eNOS pDNA. The medium dose of eNOS pDNA showed a further increase in the length density of blood vessels with an almost three-fold increase observed over the control. Interestingly, no change was observed in the length density between the 10  $\mu\text{g}$  and 20  $\mu\text{g}$  treated groups, indicating a saturation in the dose response. The 10  $\mu\text{g}$  eNOS pDNA group had the highest length density of blood vessels, but also had the lowest volume fraction of inflammatory cells, which can be linked with the fact that nitric oxide (NO) has dose-dependent anti-inflammatory properties [26]. Only the 10  $\mu\text{g}$  eNOS pDNA treated group had a statistically significant reduction in the volume fraction of inflammatory cells compared with the control, while the other groups were unchanged. This indicates that with all three doses of eNOS pDNA, the level of NO produced was not pro-inflammatory such that it could activate the pro-inflammatory NF- $\kappa$ B pathway [26]. Considering the increase observed in length density of blood vessels and the reduction in volume fraction of inflammatory cells, the 10  $\mu\text{g}$  eNOS pDNA treated group has been identified as the optimal dosing regimen.

Following on from the selection of the optimal doses of anti-inflammatory IL-6 siRNA (1  $\mu\text{g}$ ) and the pro-angiogenic eNOS pDNA (10  $\mu\text{g}$ ), these two optimal doses were combined and the tissue response, in terms of inflammatory response and angiogenesis, was examined. It was observed that at the seven-day time point, the combined delivery of IL-6 siRNA and eNOS pDNA resulted

in a volume fraction of inflammatory cells similar to that of the IL-6 siRNA delivery alone. When eNOS pDNA was delivered via the collagen delivery system, without the addition of IL-6 siRNA, there was no significant change in the volume fraction of inflammatory cells (Fig. 5A).

At 14 days, a similar pattern emerged to that which was detected at seven days. That is, addition of IL-6 siRNA to the collagen delivery system significantly reduced the volume fraction of inflammatory cells. Delivery of eNOS pDNA alone via the collagen delivery system resulted in a reduced volume fraction of inflammatory cells when compared with the control. Interestingly however, this was not to the same level as when IL-6 siRNA was delivered, and there was a significant difference between the group receiving eNOS pDNA alone and the two that received IL-6 siRNA, either without or with eNOS pDNA. Thus, it is clear that at 14 days the addition of IL-6 siRNA (with or without eNOS pDNA) significantly reduces the volume fraction of inflammatory cells.

At 7 days there was a statistically significant increase in length density of blood vessels in the eNOS pDNA treated group and the IL-6 siRNA and eNOS pDNA dual-treated group when compared with the control group, with an almost two-fold increase observed. There was no significant difference between the eNOS pDNA treated group and the IL-6 siRNA and eNOS pDNA dual-treated groups. The IL-6 siRNA treated group appeared to have a trend towards a reduction in length density of blood vessels, but no significant difference was detected. Further data on the perfusion of the tissue was acquired by measuring the average distance between adjacent blood vessels (radial diffusion distance). It was observed that eNOS pDNA treated groups, with or without IL-6 siRNA, had a significantly reduced radial diffusion distance compared with the control.

The samples at 14 days displayed a similar trend to those at 7 days. Again, length density of blood vessels was greatest in eNOS pDNA treated groups, both without and with the addition of IL-6 siRNA. The length density of blood vessels in both these groups were significantly greater than the control, while the IL-6 siRNA alone treated group was not statistically different to the control. Radial diffusion distance was also statistically different between eNOS treated groups compared with control and IL-6 siRNA alone treatment.

In order to correlate the observed anti-inflammatory and pro-angiogenic effects with a set of signals involved in pathophysiological events, a protein blot array was used to analyse the relative expression patterns of 90 proteins simultaneously. Fig. 6A shows that the delivery of IL-6 siRNA resulted in a reduction of IL-6 and a range of other pro-inflammatory factors at seven days. This reduction is in line with the reduction in volume fraction of inflammatory cells seen from stereological evaluation. A reduction was also observed in the expression of angiogenic factors. Although there was no significant difference in angiogenic parameters measured stereologically, reduction in angiogenic factors implies an alteration of the angiogenic process following IL-6 siRNA incorporation into the collagen sphere-in-hydrogel system. At 14 days, IL-6 siRNA reduced IL-6 protein expression, along with that of IP-10 and RELM- $\beta$ . Increased IL-4 and IL-13 expression are indicative of an alternative macrophage activation state, more regulatory in nature compared with classically activated macrophages, and indicative of an anti-inflammatory phenotype. This is further emphasized by increased expression of angiogenic factors (VEGF and VEGF-C) and receptors (NRP-2). However, in contrast with the groups that received eNOS pDNA treatment, the absence of an increase in PDGF-AA expression implies that blood vessels formed are likely to be immature and regress over time.

Addition of eNOS pDNA to the collagen sphere-in-hydrogel system resulted in an increased expression of a number of

angiogenic factors (bFGF, FGF-bp, CXCR4, PDGF-AA, VEGF and NRP-2). CXCR4 is the receptor for stromal-derived factor-1 (SDF-1), a key pathway in neo-angiogenesis, involved in the recruitment of endothelial precursors [57,58]. NRP-2 is a receptor for VEGF, and has been shown to interact with VEGF receptor-2 (VEGFR-2) and -3 (VEGFR-3). The increase observed in CINC-2/3 and MIP-2 shows the link between angiogenesis and inflammation, implying that increased angiogenesis will also result in an increase in inflammatory factors. This again implies the need for a combined therapy to modulate both inflammation and angiogenesis. At 14 days a similar increase in angiogenic factors was observed, with the exception of FGF and NRP-2 that are unchanged compared with the control and an increase in osteopontin (OPN) and matrix metalloproteinase-8 (MMP-8) expression. Both OPN [59,60] and MMP-8 [61] have been proven to play important roles in angiogenesis *in vitro* and *in vivo*. The reduction in IL-10 expression, coupled with no change in IL-4 and IL-13 expression, indicates macrophages may be in a more pro-inflammatory phenotype compared with the control. This is despite the reduction observed in volume fraction of inflammatory cells seen from stereological evaluation, and poses an interesting dilemma as to whether it is better to have less infiltration of inflammatory cells, or a change in their activation state to a more regulatory phenotype. Studies show that changes in the activation state of macrophages can dramatically alter the tissue response and therapeutic benefit of biomaterials therapies in the ischemic heart [62] and injured peripheral nerve [63], while macrophage phenotype plays a role in vascularization of collagen scaffolds [64].

The combination of IL-6 siRNA delivery and eNOS pDNA from the collagen sphere-in-hydrogel system resulted in modulation of the expression of both inflammatory and angiogenic factors at seven days. As shown in Fig. 6A, there is both a reduction in inflammatory factors (IL-6, TNF- $\alpha$  and GM-CSF), consistent with reduced volume fraction of inflammatory cells, and increased expression of angiogenic factors. The combined effect of IL-6 siRNA and eNOS pDNA is clearly visible in terms of protein expression, with the reduction in inflammatory factors and increase in angiogenic factors similar to that of the individual treatments alone. In this way we clearly see the combinatorial effect of dual delivery of IL-6 siRNA and eNOS pDNA through the collagen sphere-in-hydrogel system, as compared with the same system delivering either factor separately.

At 14 days, we see similar anti-inflammatory/pro-angiogenic effects. Increased expression of IL-10, along with that of IL-4 and IL-13, suggests an alternative macrophage activation, in which macrophages are more regulatory than pro-inflammatory in nature. As with the eNOS pDNA group, there was also an increase in FADD, an anti-inflammatory mediator. In terms of angiogenesis, the expression of angiogenic factors is quite consistent throughout the two time points, with factors such as VEGF and PDGF-AA prominent. This consistency is matched in terms of surface and length density of blood vessels, which remains relatively stable across time points.

In this study, Raman microspectroscopic analyses were performed on 30  $\mu$ m tissue sections, which revealed changes in the Raman patterns are associated with GAGs and PGs present in ECM. In detail, we identified increased chondroitin-4-sulfate (C4S) in the IL-6 siRNA treated-group, while chondroitin-6-sulfate was increased in all three treatment groups (IL-6 siRNA, eNOS pDNA and the combination of both) compared with the control. There was also an increase in chondroitin sulfate proteoglycans (CSPGs) in the IL-6 siRNA and eNOS pDNA combined group compared with the control (sphere-in-hydrogel system alone). The effect of ECM changes, particularly that of GAGs in the ECM, on inflammatory and angiogenic processes is established [65]. Here, following changes in

inflammation and angiogenesis in the tissue, we observed changes with regard to GAG sulfation and also GAG and PG content of the ECM using Raman microspectroscopy.

In order to confirm changes revealed by Raman microspectroscopy, we used the DMMB assay to measure total sGAG content. Relative amounts of CS and HS were determined using a specific GAG degradation method. With regards to the total sGAG content extracted from tissue, no difference was observed between groups at 7 or 14 days (see [Supplementary info](#)). However, this must be taken with the caveat that the DMMB assay measures only sulfated GAGs, and not hyaluronic acid (HA), which is non-sulfated. Low molecular weight HA or HA fragments can act as damage-associated molecular patterns (DAMPs) and trigger immune responses. However, any changes in HA cannot be detected by this method. However, although the global GAG composition in a tissue can be detected as unchanged, it is possible that the sulfation pattern changes as a consequence of physiological and pathological events or as a result of treatment. Changes of sulfation patterns are not detected by the DMMB technique, but can be observed by the capacities of GAGs to interact with growth factors. Thus, ELISA competition assays were used as a means to assess the relative binding capacities of extracted sGAGs towards two angiogenic factors, VEGF<sub>165</sub> and bFGF. At seven days, there was a significant increase in the binding of sGAG with both growth factors tested in eNOS pDNA treated groups. For VEGF<sub>165</sub> binding, it is noticeable that there is an increase in sGAG binding at seven days in the eNOS pDNA treated samples versus the control or IL-6 siRNA treated samples. Binding to bFGF shows a similar effect, with an increase observed in the eNOS pDNA treated groups compared with the control and the IL-6 siRNA alone treated groups. Previous studies have shown that the binding of growth factors by sGAGs and sGAG-mimetics potentiates and increases the activity of growth factors [36,66]. Thus, the binding studies indicate a potential 'priming' of the sGAG content of the ECM toward a more angiogenic capacity due to treatment with eNOS pDNA. However, this appeared only to be a temporal change, as by 14 days the eNOS pDNA treated samples returned to baseline for bFGF binding. Interestingly, for VEGF<sub>165</sub>, there was a greater reduction in binding with the eNOS pDNA treated samples at fourteen days. Similarly, sGAG binding of bFGF was unchanged between samples at 14 days. This may be due to the temporal nature of the angiogenic process. The early stages of angiogenesis, such as pericyte detachment, increased vascular permeability and endothelial cell proliferation, are primarily governed by VEGF<sub>165</sub> and bFGF activity [67]. However, in later stages, other factors such as platelet-derived growth factor (PDGF) and transforming growth factor- $\beta$  (TGF- $\beta$ ) are more dominant in processes such as pericyte attachment and maturation and basement membrane deposition. Thus it appears that the sGAG content of the ECM changes its affinity towards growth factors over time. In addition to the factors tested, it is likely that the sGAG affinity towards multiple factors changes over time. This may include a range of other growth factors as well as cytokines that influence the progression of both angiogenesis and inflammation. The importance of changes in ECM compositions as well as activity are known in tumour progression, where dynamic changes in the ECM influences inflammation and angiogenesis in the tumor microenvironment, promoting tumor growth [29]. Similar effects have been observed with the ECM during cardiovascular disease, where the balance between inflammation and angiogenesis is shifted [28].

## 5. Conclusions

A collagen sphere-in-hydrogel system has been developed and optimized for the delivery of IL-6 siRNA (from the hydrogel phase) to modulate inflammation and eNOS pDNA (from the microsphere

phase) to increase angiogenesis in an *in vivo* subcutaneous model. Dual delivery of the optimal IL-6 siRNA and eNOS pDNA doses through the collagen sphere-in-hydrogel system resulted in a reduction in the infiltration of inflammatory cells and an increase in blood vessels at 7 and 14 days. Protein expression analysis revealed an overall reduction in the expression of inflammatory cytokines and an increase in the expression of angiogenic factors. Raman microscopy displayed a change in the ECM of the treated tissue, particularly with regard to bands associated with GAG content and sulfation. Analysis of the total sGAG content and ratio of CS:HS following treatment revealed no changes between groups at both 7 and 14 days. However, further investigation showed a change in the binding capacity of tissue-extracted sGAG to growth factors VEGF<sub>165</sub> and bFGF, which was in line with the increase in blood vessels observed following treatment with eNOS pDNA, whether with or without co-delivery of IL-6 siRNA.

## Acknowledgements

The authors would like to acknowledge financial support from Science Foundation Ireland (Grant no. 07/SRC/B1163) and travel support from the European Molecular Biology Organisation (EMBO) and the Deutscher Akademischer Austausch Dienst (DAAD).

## Appendix A. Supplementary data

Supplementary data related to this article can be found at <http://dx.doi.org/10.1016/j.biomaterials.2015.08.012>.

## References

- [1] Elsie S. Place, Nicholas D. Evans, Molly M. Stevens, Complexity in biomaterials for tissue engineering, *Nat. Mater.* 8 (2009) 457–470, <http://dx.doi.org/10.1038/nmat2441>.
- [2] Jeffrey M. Karp, Robert Langer, Development and therapeutic applications of advanced biomaterials, *Curr. Opin. Biotechnol.* 18 (2007) 454–459, <http://dx.doi.org/10.1016/j.copbio.2007.09.008>.
- [3] Chaenyung Cha, William B. Liechty, Ali Khademhosseini, Nicholas A. Peppas, Designing biomaterial to direct stem cell fate, *ACS Nano* 6 (2012) 9353–9358.
- [4] Faramarz Adalat, Iris Sheu, Sam Manoucheri, Ali Khademhosseini, Material strategies for creating artificial cell-instructive niches, *Curr. Opin. Biotechnol.* 23 (2012) 820–825, <http://dx.doi.org/10.1016/j.copbio.2012.05.007>.
- [5] Ensanya Abou Neel, Laurent Bozec, Jonathan C. Knowles, Omaer Syed, Vivek Mudera, Richard Day, Jung Keun Hyun, Collagen – emerging collagen based therapies hit the patient, *Adv. Drug Deliv. Rev.* (2012), <http://dx.doi.org/10.1016/j.addr.2012.08.010>.
- [6] Shane Browne, Dimitrios I. Zeugolis, Abhay Pandit, Collagen – finding a solution for the source, *Tissue Eng. Part A* 19 (2013) 1491–1494.
- [7] Daniel T. Luttkhuizen, Machteld J. van Amerongen, Pieter C. de Feijter, Arjen H. Petersen, Martin C. Harmsen, Marja JA. van Luyn, The correlation between difference in foreign body reaction between implant locations and cytokine and MMP expression, *Biomaterials* 27 (2006) 5763–5770, <http://dx.doi.org/10.1016/j.biomaterials.2006.07.004>.
- [8] Qingsong Ye, Martin C. Harmsen, Yijin Ren, Ruud A. Bank, The role of collagen receptors Endo180 and DDR-2 in the foreign body reaction against non-crosslinked collagen and gelatin, *Biomaterials* 32 (2011) 1339–1350, <http://dx.doi.org/10.1016/j.biomaterials.2010.09.076>.
- [9] Qingsong Ye, Martin C. Harmsen, Marja JA. van Luyn, Ruud A. Bank, The relationship between collagen scaffold cross-linking agents and neutrophils in the foreign body reaction, *Biomaterials* 31 (2010) 9192–9201, <http://dx.doi.org/10.1016/j.biomaterials.2010.08.049>.
- [10] Martin C. Harmsen, Marja JA. Luyn, Cellular and molecular dynamics in the foreign body reaction, *Tissue Eng.* (2006) 12.
- [11] Eliane R. Poppa, Martin C. Harmsen, Rene A. Tio, Barry WA. van der Strate, Linda A. Brouwer, Martin Schipper, Jasper Koerts, Mike J.L. De Jongste, Aldert Hazenberg, Marc Hendriks, Marja JA. van Luyn, Circulating CD34+ progenitor cells modulate host angiogenesis and inflammation *in vivo*, *J. Mol. Cell. Cardiol.* 41 (2006) 86–96, <http://dx.doi.org/10.1016/j.yjmcc.2006.04.021>.
- [12] Douglas M. Noonan, Andrea De Lerma Barbaro, Nicola Vannini, Lorenzo Mortara, Adriana Albini, Inflammation, inflammatory cells and angiogenesis: decisions and indecisions, *Cancer Metastasis Rev.* 27 (2008) 31–40, <http://dx.doi.org/10.1007/s10555-007-9108-5>.
- [13] Matthew J. Webber, John B. Matson, Vibha K. Tamboli, Samuel I. Stupp, Controlled release of dexamethasone from peptide nanofiber gels to modulate inflammatory response, *Biomaterials* 33 (2012) 6823–6832, <http://dx.doi.org/10.1016/j.biomaterials.2012.06.003>.
- [14] Anne Des Rieux, Bernard Ucakar, Billy Paul Kaishusha Mupendwa, Didier Colau, Olivier Feron, Peter Carmeliet, Véronique Préat, 3D systems delivering VEGF to promote angiogenesis for tissue engineering, *J. Control. Release* 150 (2011) 272–278, <http://dx.doi.org/10.1016/j.jconrel.2010.11.028>.
- [15] S.M. Van Putten, M. Wübben, W.E. Hennink, M.J.A. van Luyn, M.C. Harmsen, The downmodulation of the foreign body reaction by cytomegalovirus encoded interleukin-10, *Biomaterials* 30 (2009) 730–735, <http://dx.doi.org/10.1016/j.biomaterials.2008.10.043>.
- [16] Christoph Heidenhain, Ariyakhagorn Veeravoorn, Blagovest Vachkov, Wilko Weichert, Gerhard Schmidmaier, Britt Wildemann, Peter Neuhaus, Michael Heise, Fibroblast and vascular endothelial growth factor coating of decellularized vascular grafts stimulates undesired giant cells and graft encapsulation in a rat model, *Artif. Organs* 35 (2011) E1–E10, <http://dx.doi.org/10.1111/j.1525-1594.2010.01072.x>.
- [17] Sandra I. Zittermann, Andrew C. Issekutz, Endothelial growth factors VEGF and bFGF differentially enhance monocyte and neutrophil recruitment to inflammation, *J. Leukoc. Biol.* 80 (2006) 247–257, <http://dx.doi.org/10.1189/jlb.1205718.1>.
- [18] S. Browne, A. Pandit, Multi-modal delivery of therapeutics using biomaterial scaffolds, *J. Mater. Chem. B* 2 (2014) 6692–6707, <http://dx.doi.org/10.1039/C4TB00863D>.
- [19] Jennifer C. Alexander, Shane Browne, Abhay Pandit, Yury Rochev, Biomaterial constructs for delivery of multiple therapeutic genes: a spatiotemporal evaluation of efficacy using molecular beacons, *PLoS One* 8 (2013) e65749, <http://dx.doi.org/10.1371/journal.pone.0065749>.
- [20] Mercedes Rincon, Interleukin-6: from an inflammatory marker to a target for inflammatory diseases, *Trends Immunol.* 33 (2012) 571–577, <http://dx.doi.org/10.1016/j.it.2012.07.003>.
- [21] Gilles Kaplanski, Valérie Marin, Félix Montero-Julian, Alberto Mantovani, Catherine Farnarier, IL-6: a regulator of the transition from neutrophil to monocyte recruitment during inflammation, *Trends Immunol.* 24 (2003) 25–29.
- [22] Jürgen Scheller, Athena Chalaris, Dirk Schmidt-Arras, Stefan Rose-John, The pro- and anti-inflammatory properties of the cytokine interleukin-6, *Biochim. Biophys. Acta* 1813 (2011) 878–888, <http://dx.doi.org/10.1016/j.bbamcr.2011.01.034>.
- [23] Dan G. Duda, Dai Fukumura, Rakesh K. Jain, Role of eNOS in neo-vascularization: NO for endothelial progenitor cells, *Trends Mol. Med.* 10 (2004) 143–145.
- [24] Thomas Michel, NO way to relax: the complexities of coupling nitric oxide synthase pathways in the heart, *Circulation* 121 (2010) 484–486, <http://dx.doi.org/10.1161/CIR.0b013e3181d1e24e>.
- [25] Charles D. Searles, The nitric oxide pathway and oxidative stress in heart failure, *Congest. Heart Fail.* 8 (2002), 142–7, 155.
- [26] Jakub Siednienko, Joanna Nowak, Paul N. Moynagh, Wojciech A. Gorczyca, Nitric oxide affects IL-6 expression in human peripheral blood mononuclear cells involving GMP-dependent modulation of NF-κB activity, *Cytokine* 54 (2011) 282–288, <http://dx.doi.org/10.1016/j.cyto.2011.02.015>.
- [27] Christian Frantz, Kathleen M. Stewart, Valerie M. Weaver, The extracellular matrix at a glance, *J Cell Sci.* (2010) 4195–4200, <http://dx.doi.org/10.1242/jcs.023820>.
- [28] Alicia G. Arroyo, M Luisa Iruela-Arispe, Extracellular matrix, inflammation, and the angiogenic response, *Cardiovasc. Res.* 86 (2010) 226–235, <http://dx.doi.org/10.1093/cvr/cvq049>.
- [29] Pengfei Lu, Valerie M. Weaver, Zena Werb, The extracellular matrix: a dynamic niche in cancer progression, *J. Cell. Biol.* 196 (2012) 395–406, <http://dx.doi.org/10.1083/jcb.201102147>.
- [30] Junko Iijima, Kenjiro Konno, Naoki Iitano, Inflammatory alterations of the extracellular matrix in the tumor microenvironment, *Cancers (Basel)* 3 (2011) 3189–3205, <http://dx.doi.org/10.3390/cancers3033189>.
- [31] Eva Brauchle, Hannah Johannsen, Samantha Nolan, Sibylle Thude, Katja Schenke-Layland, Design and analysis of a squamous cell carcinoma *in vitro* model system, *Biomaterials* 34 (2013) 7401–7407, <http://dx.doi.org/10.1016/j.biomaterials.2013.06.016>.
- [32] Marieke Pudlas, Eva Brauchle, Travis J. Klein, Dietmar W. Hutmacher, Katja Schenke-Layland, Non-invasive identification of proteoglycans and chondrocyte differentiation state by Raman microspectroscopy, *J. Biophot.* 6 (2013) 205–211, <http://dx.doi.org/10.1002/jbio.201200064>.
- [33] Ram Sasisekharan, Rahul Raman, Vikas Prabhakar, Glycomics approach to structure-function relationships of glycosaminoglycans, *Annu. Rev. Biomed. Eng.* 8 (2006) 181–231, <http://dx.doi.org/10.1146/annurev.bioeng.8.061505.095745>.
- [34] Kristen R. Taylor, Richard L. Gallo, Glycosaminoglycans and their proteoglycans: host-associated molecular patterns for initiation and modulation of inflammation, *FASEB J.* 20 (2006) 9–22, <http://dx.doi.org/10.1096/fj.05-4682rev>.
- [35] Neha S. Gandhi, Ricardo L. Mancera, The structure of glycosaminoglycans and their interactions with proteins, *Chem. Biol. Drug Des.* 72 (2008) 455–482, <http://dx.doi.org/10.1111/j.1747-0285.2008.00741.x>.
- [36] Minh Bao Huynh, Christophe Morin, Gilles Carpentier, Stephanie Garcia-Filipe, Sofia Talhas-Perret, Véronique Barbier-Chassefière, Toin H. van Kuppevelt, Isabelle Martelly, Patricia Albanese, Dulce Papy-Garcia, Age-related changes in rat myocardium involve altered capacities of glycosaminoglycans to potentiate growth factor functions and heparan sulfate-altered sulfation, *J. Biol.*

- Chem. 287 (2012) 11363–11373, <http://dx.doi.org/10.1074/jbc.M111.335901>.
- [37] D.I. Zeugolis, R.G. Paul, G. Attenburrow, Factors influencing the properties of reconstituted collagen fibers prior to self-assembly: animal species and collagen extraction method, *J. Biomed. Mater. Res. A* 86 (2008) 892–904, <http://dx.doi.org/10.1002/jbma.a.31694>.
- [38] Shane Browne, Gianluca Fontana, Brian J. Rodriguez, Abhay Pandit, A protective extracellular matrix-based gene delivery reservoir fabricated by electrostatic charge manipulation, *Mol. Pharm.* 9 (2012) 3099–3106, <http://dx.doi.org/10.1021/mp300231d>.
- [39] Michael Monaghan, Shane Browne, Katja Schenke-Layland, Abhay Pandit, A collagen-based scaffold delivering exogenous microRNA-29B to modulate extracellular matrix remodeling, *Mol. Ther.* 22 (2014) 786–796, <http://dx.doi.org/10.1038/mt.2013.288>.
- [40] Carolyn Holladay, Karen Power, Michael Sefton, Timothy O'Brien, William M. Gallagher, Abhay Pandit, Functionalized scaffold-mediated interleukin 10 gene delivery significantly improves survival rates of stem cells in vivo, *Mol. Ther.* 19 (2011) 969–978, <http://dx.doi.org/10.1038/mt.2010.311>.
- [41] Yolanda Garcia, Ailish Breen, Krishna Burugapalli, Peter Dockery, Abhay Pandit, Stereological methods to assess tissue response for tissue-engineered scaffolds, *Biomaterials* 28 (2007) 175–186, <http://dx.doi.org/10.1016/j.biomaterials.2006.08.037>.
- [42] Miriam Votteler, Daniel A Carvajal Berrio, Alexander Horke, Laetitia Sabatier, Dieter P. Reinhardt, Ali Nsair, Elena Aikawa, Katja Schenke-Layland, Elastogenesis at the onset of human cardiac valve development, *Development* 140 (2013) 2345–2353, <http://dx.doi.org/10.1242/dev.093500>.
- [43] Marieke Pudlas, Daniel Alejandro Carvajal Berrio, Miriam Votteler, Steffen Koch, Sibylle Thude, Heike Walles, Katja Schenke-Layland, Non-contact discrimination of human bone marrow-derived mesenchymal stem cells and fibroblasts using Raman spectroscopy, *Med. Laser Appl.* 26 (2011) 119–125, <http://dx.doi.org/10.1016/j.mla.2011.05.004>.
- [44] Eva Brauchle, Sibylle Thude, Sara Y. Brucker, Katja Schenke-Layland, Cell death stages in single apoptotic and necrotic cells monitored by Raman microspectroscopy, *Sci. Rep.* 4 (2014) 4698, <http://dx.doi.org/10.1038/srep04698>.
- [45] S. Najjam, R.V. Gibbs, M.Y. Gordon, C.C. Rider, Characterization of human recombinant interleukin 2 binding to heparin and heparan sulfate using an ELISA approach, *Cytokine* 9 (1997) 1013–1022, <http://dx.doi.org/10.1006/cyto.1997.0246>.
- [46] Julie A. Champion, Amanda Walker, Samir Mitragotri, Role of particle size in phagocytosis of polymeric microspheres, *Pharm. Res.* 25 (2008) 1815–1821, <http://dx.doi.org/10.1007/s11095-008-9562-y>.
- [47] Nishit Doshi, Samir Mitragotri, Macrophages recognize size and shape of their targets, *PLoS One* 5 (2010) e10051, <http://dx.doi.org/10.1371/journal.pone.0010051>.
- [48] Christophe Helary, Shane Browne, Asha Mathew, Wenxin Wang, Abhay Pandit, Transfection of macrophages by collagen hollow spheres loaded with polyplexes: a step towards modulating inflammation, *Acta Biomater.* 8 (2012) 4208–4214, <http://dx.doi.org/10.1016/j.actbio.2012.06.017>.
- [49] James M. Anderson, Analiz Rodriguez, David T. Chang, Foreign body reaction to biomaterials, *Semin. Immunol.* 20 (2008) 86–100, <http://dx.doi.org/10.1016/j.smim.2007.11.004>.
- [50] Maria Ruweka Fernando, Jose Luis Reyes, Jordan Iannuzzi, Gabriella Leung, Derek Mark McKay, The pro-inflammatory cytokine, interleukin-6, enhances the polarization of alternatively activated macrophages, *PLoS One* 9 (2014) e94188, <http://dx.doi.org/10.1371/journal.pone.0094188>.
- [51] Feifei Ma, Yulin Li, Lixin Jia, Yalei Han, Jizhong Cheng, Huihua Li, Yongfen Qi, Jie Du, Macrophage-stimulated cardiac fibroblast production of IL-6 is essential for TGF  $\beta$ /Smad activation and cardiac fibrosis induced by angiotensin II, *PLoS One* 7 (2012) e35144, <http://dx.doi.org/10.1371/journal.pone.0035144>.
- [52] Lin-Hung Wei, Min-Liang Kuo, Chi-An Chen, Chia-Hung Chou, Kuo-Bau Lai, Chien-Nan Lee, Chang-Yao Hsieh, Interleukin-6 promotes cervical tumor growth by VEGF-dependent angiogenesis via a STAT3 pathway, *Oncogene* 22 (2003) 1517–1527, <http://dx.doi.org/10.1038/sj.onc.1206226>.
- [53] B. Motro, A. Itin, L. Sachs, E. Keshet, Pattern of interleukin 6 gene expression in vivo suggests a role for this cytokine in angiogenesis, *Proc. Natl. Acad. Sci. U. S. A.* 87 (1990) 3092–3096.
- [54] Hyun-Ji Park, Fan Yang, Seung-Woo Cho, Nonviral delivery of genetic medicine for therapeutic angiogenesis, *Adv. Drug Deliv. Rev.* 64 (2012) 40–52, <http://dx.doi.org/10.1016/j.addr.2011.09.005>.
- [55] Mangesh Kulkarni, Aonghus O. Loughlin, R. Vazquez, K. Mashayekhi, Peadar Rooney, Udo Greiser, E.O. Toole, T.O. Brien, Maria M. Malagon, A. Pandit, Use of a fibrin-based system for enhancing angiogenesis and modulating inflammation in the treatment of hyperglycemic wounds, *Biomaterials* 35 (2014) 2001–2010.
- [56] Ailish Breen, Peter Dockery, Timothy O'Brien, Abhay Pandit, The use of therapeutic gene eNOS delivered via a fibrin scaffold enhances wound healing in a compromised wound model, *Biomaterials* 29 (2008) 3143–3151, <http://dx.doi.org/10.1016/j.biomaterials.2008.04.020>.
- [57] Hao Zheng, Tao Dai, Binquan Zhou, Junhui Zhu, He Huang, Min Wang, Guosheng Fu, SDF-1 $\alpha$ /CXCR4 decreases endothelial progenitor cells apoptosis under serum deprivation by PI3K/Akt/eNOS pathway, *Atherosclerosis* 201 (2008) 36–42, <http://dx.doi.org/10.1016/j.atherosclerosis.2008.02.011>.
- [58] Isabelle Petit, David Jin, Shahin Rafii, The SDF-1-CXCR4 signaling pathway: a molecular hub modulating neo-angiogenesis, *Trends Immunol.* 28 (2007) 299–307, <http://dx.doi.org/10.1016/j.it.2007.05.007>.
- [59] E.E. Vaughan, A. Liew, K. Mashayekhi, P. Dockery, J. McDermott, B. Kealy, A. Flynn, A. Duffy, C. Coleman, A. O'Regan, F.P. Barry, T. O'Brien, Pre-treatment of endothelial progenitor cells with osteopontin enhances cell therapy for peripheral vascular disease, *Cell Transpl.* (2012), <http://dx.doi.org/10.3727/096368911X623880>.
- [60] Aonghus O. Loughlin, Mangesh Kulkarni, Erin E. Vaughan, Michael Creane, Aaron Liew, Peter Dockery, Abhay Pandit, Timothy O. Brien, Autologous circulating angiogenic cells treated with osteopontin and delivered via a collagen scaffold enhance wound healing in the alloxan-induced diabetic rabbit ear ulcer model, *Stem Cell Res. Ther.* 4 (2013) 1–14.
- [61] Changcun Fang, Guanmei Wen, Li Zhang, Luyang Lin, Andrew Moore, Shuming Wu, Shu Ye, Qingzhong Xiao, An important role of matrix metalloproteinase-8 in angiogenesis in vitro and in vivo, *Cardiovasc. Res.* 99 (2013) 146–155, <http://dx.doi.org/10.1093/cvr/cvt060>.
- [62] Carolyn A. Holladay, Aoife M. Duffy, Xizhe Chen, Michael V. Sefton, Timothy D. O'Brien, Abhay S. Pandit, Recovery of cardiac function mediated by MSC and interleukin-10 plasmid functionalised scaffold, *Biomaterials* 33 (2012) 1303–1314, <http://dx.doi.org/10.1016/j.biomaterials.2011.10.019>.
- [63] Nassir Mokarram, Alishah Merchant, Vivek Mukhatyar, Gaurang Kumar Patel, Ravi V. Bellamkonda, Effect of modulating macrophage phenotype on peripheral nerve repair, *Biomaterials* 33 (2012) 8793–8801, <http://dx.doi.org/10.1016/j.biomaterials.2012.08.050>.
- [64] Kara L. Spiller, Rachel R. Anfang, Krista J. Spiller, Johnathan Ng, Kenneth R. Nakazawa, Jeffrey W. Daulton, Gordana Vunjak-Novakovic, The role of macrophage phenotype in vascularization of tissue engineering scaffolds, *Biomaterials* 35 (2014) 4477–4488, <http://dx.doi.org/10.1016/j.biomaterials.2014.02.012>.
- [65] Alicia G. Arroyo, M Luisa Iruela-Arispe, Extracellular matrix, inflammation, and the angiogenic response, *Cardiovasc. Res.* 86 (2010) 226–235, <http://dx.doi.org/10.1093/cvr/cvq049>.
- [66] Vincent Rouet, Yamina Hamma-Kourbali, Emmanuel Petit, Panagiota Panagopoulou, Panagiotis Katsoris, Denis Barritault, Jean-Pierre Caruelle, José Courty, A synthetic glycosaminoglycan mimetic binds vascular endothelial growth factor and modulates angiogenesis, *J. Biol. Chem.* 280 (2005) 32792–32800, <http://dx.doi.org/10.1074/jbc.M504492200>.
- [67] M.J. Cross, L. Claesson-Welsh, FGF and VEGF function in angiogenesis: signalling pathways, biological responses and therapeutic inhibition, *Trends Pharmacol. Sci.* 22 (2001) 201–207.